

Asiago eclipsing binaries program. I. V432 Aur

A.Siviero^{1,2}, U.Munari^{2,3}, R.Sordo², S.Dallaporta⁴, T.Zwitter⁵, P.M.Marrese^{1,2}, and E.F.Milone⁶

¹ Dipartimento di Astronomia dell’Università di Padova, Osservatorio Astrofisico, 36012 Asiago (VI), Italy

² Osservatorio Astronomico di Padova, Sede di Asiago, 36012 Asiago (VI), Italy

³ CISAS, Centro Interdipartimentale Studi ed Attività Spaziali dell’Università di Padova

⁴ Via Filzi 9, I-38034 Cembra (TN), Italy

⁵ University of Ljubljana, Department of Physics, Jadranska 19, 1000 Ljubljana, Slovenia

⁶ Physics and Astronomy Department, University of Calgary, Calgary T2N 1N4, Canada

Received date; accepted date

Abstract. The orbit and physical parameters of the previously unsolved eclipsing binary V432 Aur, discovered by Hipparcos, have been derived with errors better than 1% from extensive Echelle spectroscopy and B , V photometry. Synthetic spectral analysis of both components has been performed, yielding T_{eff} and $\log g$ in close agreement with the orbital solution, a metallicity $[\text{Z}/\text{Z}_{\odot}] = -0.6$ and rotational synchronization for both components. Direct comparison on the theoretical L, T_{eff} plane with the Padova evolutionary tracks and isochrones for the masses of the two components (1.22 and 1.08 M_{\odot}) provides a perfect match and a 3.75 Gyr age. The more massive and cooler component is approaching the base of the giant branch and displays a δ Sct pulsation activity with an amplitude of $\Delta V = 0.075$ mag and $\Delta \text{rad.vel.} = 1.5 \text{ km sec}^{-1}$. With a $T_{\text{eff}} = 6080 \text{ K}$ it is one of the coolest δ Sct known, falling well to the red of the instability strip edge. Orbital modeling reveals a large and bright surface spot on it. The pulsations activity and the large spot(s) suggest the presence of wide macro-turbulent motions in its atmosphere. They reflect in a line broadening that at cursory inspection could be taken as indication of a rotation *faster* than synchronization, something obviously odd for an old, expanding star.

Key words. stars: fundamental parameters – binaries: spectrophotometric – binaries: eclipsing – pulsating stars – stellar spots star: individual: V432 Aur

1. Introduction

Eclipsing binaries are a recognized high performance tool to derive fundamental stellar parameters (like masses and radii), and as such they play a key astrophysical role over the whole HR diagram (cf. Andersen 1991). They also provide a *geometrical* distance determination, and comparison with Hipparcos parallaxes supports this statement. The more accurate the data and sophisticated the analysis, the closer the match with Hipparcos parallaxes, usually within just a few per cent. Eclipsing binaries also offer the possibility to *close the loop* with, for example, techniques of synthetic spectroscopy. The synthetic modeling of spectra of SB2 eclipsing binaries at quadrature (for ex. via Kurucz, MARCS, NextGen, and other families of model atmospheres and synthetic spectra) allows to derive fundamental parameters like temperature and surface gravity that can be directly compared with the results of the orbital modeling.

With this paper we begin a series of papers aimed to present the results obtained on a number of SB2 eclipsing

binaries selected among those missing a solution in literature, or with improvable results. For the program stars we have obtained accurate photoelectric or CCD photometry, generally in B and V bands of the Johnson system, and high S/N, high resolution (resolving power 20000) Echelle+CCD spectroscopy over the whole 4550-9480 Å range. The goal is to provide accurate orbital solutions and stellar parameters, analyze the stellar atmospheres via synthetic spectra techniques and derive evolutionary status and age via comparison with evolutionary stellar models and tracks. A further goal is to provide the proper reference against which to judge the accuracy obtainable on SB2 eclipsing binaries by the ESA’s GAIA mission to be launched in 2010, a GAIA-like orbital solution being already obtained elsewhere for the majority of the systems considered in this series (e.g. Munari et al. 2001, Zwitter et al. 2003).

We open this series of papers with V432 Aur, a late F double lined eclipsing binary discovered as an “unsolved” variable by Hipparcos. We have already obtained accurate B and V photometry of V432 Aur discovering that it is a fine eclipsing binary with a 3.1 day orbital period, and

Table 1. Heliocentric radial velocities of V432 Aur. The columns give the spectrum number (from the Asiago Echelle log book), the orbital phase according to Dallaporta et al. 2002b, the heliocentric JD (-2452000), the radial velocities of the two components and the corresponding errors, and the $\langle S/N \rangle$ of the spectrum averaged over the six Echelle orders considered in the analysis.

#	Phase	HJD	Star 1		Star 2		$\langle S/N \rangle$
			RV_{\odot}	ϵ	RV_{\odot}	ϵ	
39643	0.088	690.3589	-43.3	0.8	58.2	0.5	190
39653	0.122	690.4646	-57.7	0.9	73.8	0.5	200
39046	0.125	505.5673	-59.7	0.6	75.5	1.4	190
39655	0.131	690.4904	-62.0	1.1	76.7	0.7	200
39821	0.170	718.3465	-80.0	0.8	90.5	0.3	190
39823	0.178	718.3724	-80.7	1.6	91.2	0.5	220
39826	0.195	718.4247	-84.0	1.2	95.8	0.5	160
37947	0.203	302.4140	-87.7	1.6	97.0	0.7	140
39721	0.205	712.2929	-87.8	1.4	97.2	0.6	140
39235	0.234	598.3553	-91.2	1.2	100.5	0.5	100
39233	0.237	598.3553	-91.7	1.6	99.6	0.7	120
39237	0.251	598.4079	-92.2	1.3	99.8	0.8	90
39239	0.259	598.4336	-90.7	1.2	102.1	0.7	120
39241	0.267	598.4590	-90.7	1.2	100.8	0.7	80
39247	0.282	598.5042	-86.7	1.8	100.1	0.9	80
39249	0.290	598.5297	-89.2	1.3	98.3	0.6	130
39251	0.299	598.5551	-88.0	1.1	95.3	0.6	130
39225	0.308	595.5037	-82.7	1.4	96.7	0.6	160
38387	0.333	361.3665	-76.8	2.6	90.3	0.7	60
39310	0.333	629.4800	-74.5	1.6	90.7	0.6	100
38389	0.339	361.3854	-75.2	2.1	87.3	0.8	60
39312	0.342	629.5060	-72.8	1.1	87.2	0.5	80
38302	0.353	358.3482	-71.8	1.3	79.7	0.8	140
39314	0.357	629.5523	-68.0	1.1	82.5	1.4	90
39864	0.502	719.3694			10.5	0.2	170
39866	0.511	719.3971			4.7	0.2	150
38414	0.649	362.3391	92.0	0.7	-62.7	0.6	140
39272	0.660	627.4048	97.2	0.7	97.2	0.7	120
39274	0.668	627.4305	99.4	0.2	-68.2	0.6	160
39276	0.677	627.4560	103.1	0.2	-70.3	0.6	160
39278	0.685	627.4831	103.6	0.5	-72.9	0.8	160
39280	0.694	627.5097	106.9	0.4	-73.6	0.6	160
39282	0.702	627.5352	107.2	0.6	-76.9	0.7	170
39290	0.734	627.6334	113.6	0.5	-77.7	0.7	190
39292	0.743	627.6596	112.4	0.9	-79.3	0.6	170
39605	0.745	689.3010	111.6	0.9	-80.9	0.7	220
39294	0.751	627.6852	112.1	0.9	-79.8	0.7	200
39607	0.753	689.3270	111.3	0.8	-80.8	0.7	190
39617	0.799	689.4682	106.3	0.6	-76.2	0.2	160
39026	0.807	504.5867	104.8	0.7	-74.5	0.8	130
39619	0.807	689.4942	104.3	0.9	-76.0	0.2	150
39028	0.813	504.6057	105.1	0.4	-73.3	0.6	90
39076	0.864	566.3983	82.8	1.0	-60.2	1.1	115
39077	0.872	566.4226	81.8	1.5	-54.7	1.1	110
39078	0.880	566.4466	78.5	1.8	-52.8	0.8	150
38198	0.894	332.2787	73.2	1.3	-45.0	0.6	130
39084	0.894	566.4922	71.5	1.7	-44.2	1.1	115
39085	0.902	566.5153	68.8	1.3	-41.8	0.0	175
39086	0.909	566.5383	65.5	1.2	-39.7	0.8	180
38216	0.933	332.4002	36.6	0.9	-31.0	0.9	140

Table 2. Epoch of photometric minima of V432 Aur.

primary	secondary
2451463.561	2452574.522
2451571.413	

with one of the components being an intrinsic variable (Dallaporta et al. 2002b, hereafter Da02b). With this information derived from photometry in hand we began to obtain spectroscopic observations. This paper presents a complete analysis of the combined photometric and spectroscopic data.

2. The data

2.1. Photometry

Photometric B and V data are those already described in detail by Da02b, that used an Optec SSP5 photoelectric photometer housing standard Johnson filters. Here we augment the photometric data by an additional set obtained, exactly in the same way, around the secondary eclipse to investigate the long term photometric stability of the system and to check in more detail the reduction of intrinsic variability during the secondary eclipse. The whole set of photometric data are available in electronic form¹. In all, 1139 points in B and 1574 in V densely map the whole lightcurve, with a r.m.s. accuracy of 5 millimag.

The photometric data reported by Da02b were reduced using $V_J=8.15$, $B_J=8.85$ from Hipparcos Catalogue for the comparison star HD 36974. They have been now reduced (and as such used in the paper and listed in the web page) using the Tycho values $V_T=8.259$, $B_T=9.030$ transformed to corresponding Johnson values $V_J=8.180$, $B_J=8.871$ following the Bessell (2000) transformations.

2.2. Spectroscopy

Spectra of V432 Aur have been secured with the Echelle+CCD spectrograph on the 1.82 m telescope operated by Osservatorio Astronomico di Padova atop Mt. Ekar (Asiago). A 2 arcsec slit was adopted with fixed E-W orientation, producing a PSF with a FWHM of 1.75 pixels over the whole observing campaign, corresponding to a resolving power close to 20000. The PSF is measured on the night-sky emission lines. Even if uniformly illuminating the slit, they are considered a fair approximation of the stellar illumination mode of the slit given the typical seeing (around 2 arcsec) and the manual guiding of the star on the slit for half an hour each exposure. Analysis of isolated telluric absorption lines confirms the value for the resolving power.

¹ at <http://ulisse.pd.astro.it/Binaries/V432-Aur/>

The detector has been a UV coated Thompson CCD 1024x1024 pixel, 19 micron square size, covering in one exposure from 4500 to 9480 Å (from Echelle order #49 to #24). The short wavelength limit is set by a 2 mm OG 455 long-pass filter, inserted in the optical train to cut the second order from the cross-disperser. The wavelength range is covered without gaps between adjacent Echelle orders up to 7300 Å.

The exposure time has been 1800 sec for 45 spectra in Table 1 and 1200 sec for the remaining 7, which guaranteed an excellent S/N of the recorded spectrum while the orbital phase smearing being completely negligible (1800 sec corresponding to 0.67% of the orbital period).

The spectra have been extracted and calibrated in a standard fashion with IRAF running under Linux operating system. The wavelength solution has been derived simultaneously for all 26 recorded Echelle orders, with an average r.m.s of 0.18 km sec⁻¹. A pruned Thorium line list has been adopted, where all lines falling into blend at our 20 000 resolving power or approaching/reaching saturation at our 3 sec exposure time have been deleted, leaving an average of 11 lines per order retained in the wavelength solution.

2.3. Radial velocities

To derive the radial velocities, we have considered only the six Echelle orders #40–45 that cover the 4890–5690 Å range, trimming 25% at both ends of each order (thus retaining the central 50% of order). The reasons for this are: (a) at these wavelengths the target spectral energy distribution and the instrumental response reach the maximum efficiency, (b) the selected spectral range is packed with a great number of marked and similar intensity FeI lines that assure easy splitting of individual components and a great cross-correlation performance (adding further Echelle orders to the radial velocity measurements does not appreciably increase the already high accuracy of the results, requiring an unjustified extra measurement effort), (c) the trimmed six Echelle orders fall right at the center of the spectrograph focal plane and CCD imaging area, where the recorded instrumental PSF is the sharpest, (d) retaining only the central 50% of each of the six orders avoids degradation of wavelength solution accuracy towards the orders' ends and so maintains the accuracy of derived radial velocities, and (e) due to the Echelle blaze function, the instrument response at orders edges falls below 40% of the peak value at center of each order, thus producing toward order edges both a poorer S/N and a steeper continuum (harder to normalize to unity before to run the cross-correlation). The selected wavelength interval includes the $\Delta\lambda=45$ Å range centered at 5187 Å where the highly successful CfA Speedometers have been deriving accurate radial velocities for two decades now, including a wealth of binaries, as described by Latham (2002, and references therein).

Table 3. Orbital solution for V432 Aur (over-plotted to observed data in Figure 1). Formal errors of the solution are given. The last two lines compare the Hipparcos trigonometric parallax (and its 1σ error interval) with the distance derived from the orbital solution.

P (d)	3.0817438	±	0.0000014
T_0 (HJD)	2451571.41150	±	0.00027
a (R _⊕)	11.749	±	0.027
V_γ (km sec ⁻¹)	10.22	±	0.002
$q = \frac{m_2}{m_1}$	1.133	±	0.005
i (°)	90.0	±	0.9
e	0.00		
ω	0.00		
T_1 (K)	6685	±	85
T_2 (K)	6080	±	85
Ω_1	10.712	±	0.027
Ω_2	6.366	±	0.024
R_1 (R _⊕)	1.230	±	0.006
R_2 (R _⊕)	2.460	±	0.020
M_1 (M _⊕)	1.080	±	0.014
M_2 (M _⊕)	1.220	±	0.018
$M_{bol,1}$	3.710	±	0.016
$M_{bol,2}$	2.610	±	0.024
$\log g_1$ (cgs)	4.290	±	0.008
$\log g_2$ (cgs)	3.740	±	0.010
$R_{1,pole}$ (R _⊕)	1.226	±	0.004
$R_{1,point}$ (R _⊕)	1.230	±	0.004
$R_{1,side}$ (R _⊕)	1.227	±	0.004
$R_{1,back}$ (R _⊕)	1.229	±	0.004
$R_{2,pole}$ (R _⊕)	2.440	±	0.011
$R_{2,point}$ (R _⊕)	2.498	±	0.012
$R_{2,side}$ (R _⊕)	2.461	±	0.011
$R_{2,back}$ (R _⊕)	2.489	±	0.012
d_{Hip} (pc)	118 ₁₄₆ ¹⁰⁰		
d_{orb} (pc)	134	±	3

Radial velocities were measured with the two-dimensional correlation algorithm `todcor` (Zucker and Mazeh 1994). This is a multiple correlation technique that obtains the Doppler shifts (and the intensity ratio) of the two stellar components simultaneously. It allows for efficient solution of even blended spectra of the two stars with an unknown intensity ratio. The algorithm has been coded by us into a custom IRAF script which makes use of the Fourier correlation routine `xcsao` within the `rvsao` package (Kurtz and Mink 1998, Tonry and Davis 1979) and builds on a Fortran code kindly supplied by D. Latham. The code uses template spectra of the two stars as input. The appropriate templates have been selected among the large synthetic spectral database computed at 20 000 resolving power with Kurucz's codes by Munari et al. (2003).

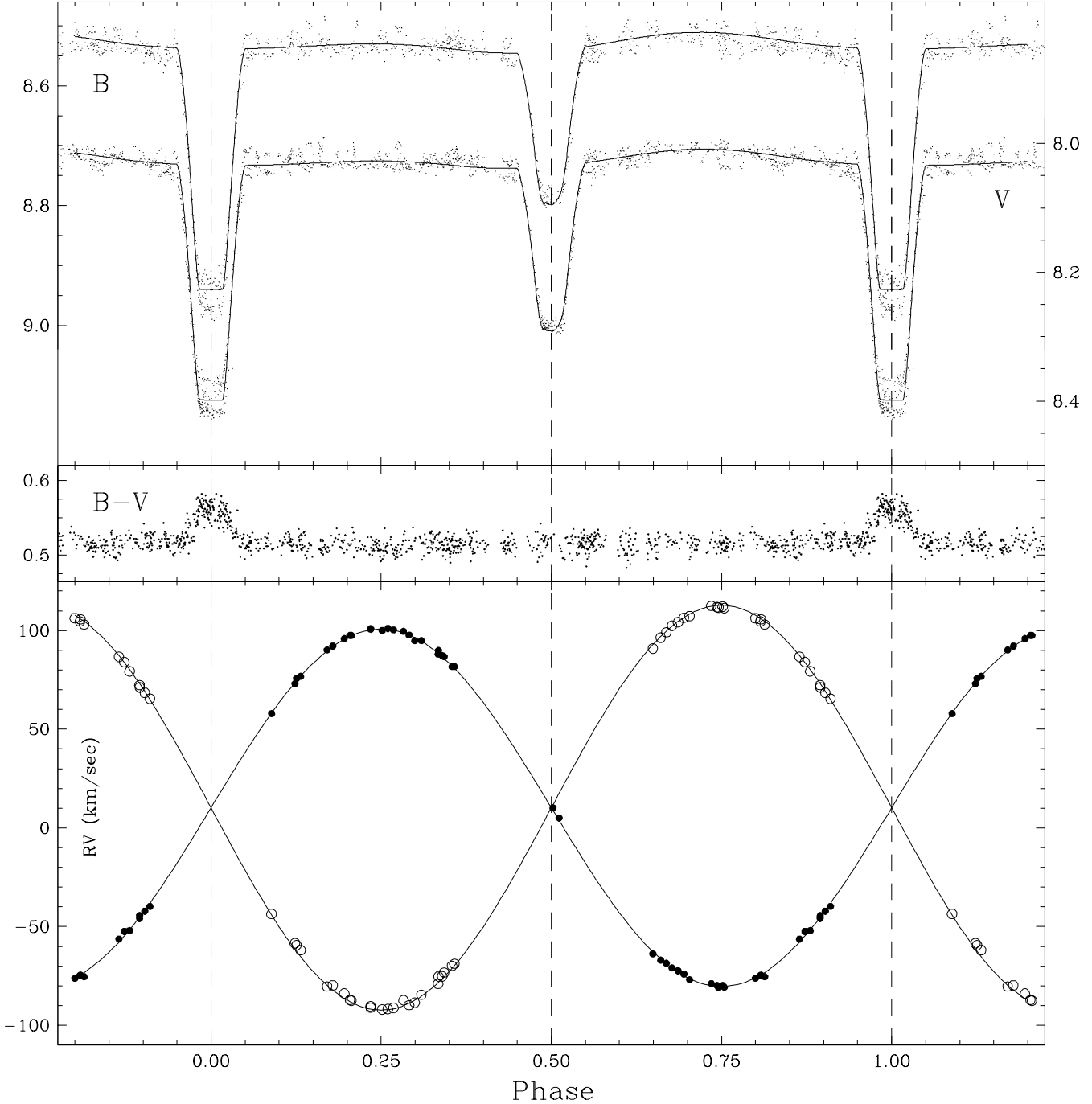


Fig. 1. The observed V , B , $B-V$ and radial velocity curves of V432 Aur with over-plotted the orbital solution given in Table 3.

A subsection of the synthetic atlas, useful for F and G main sequence stars and covering the 46 Asiago Echelle orders from 3200 to 9480 Å is available electronically to interested users². The accuracy of the radial velocities from the six selected and trimmed Echelle orders has turned

out to be constant over all six selected orders. Averaged results are summarized in Table 1. The mean error of radial velocities is 1.05 km sec^{-1} for star 1 (the fainter of the two), and 0.66 km sec^{-1} for star 2. The selected templates have been $T_{\text{eff}}=6500 \text{ K}$, $\log g=4.5$, $[Z/Z_{\odot}]=-0.5$ and $V_{\text{rot}}=20 \text{ km sec}^{-1}$ for star 1, and $T_{\text{eff}}=6250 \text{ K}$, $\log g=4.0$, $[Z/Z_{\odot}]=-0.5$ and $V_{\text{rot}}=40 \text{ km sec}^{-1}$ for star 2.

² http://ulisse.pd.astro.it/Binaries/cross_corr/.

The grid (fits files) covers temperatures from 7500 to 5000 K for $\log g=4.5$ (corresponding to main sequence stars from A9 to K0), metallicities $[Z/Z_{\odot}]=-1.0, -0.5, 0.0$ and rotational velocities of 0, 5, 10, 15, 20, 30, 40, 50, 75, 100 km sec^{-1} .

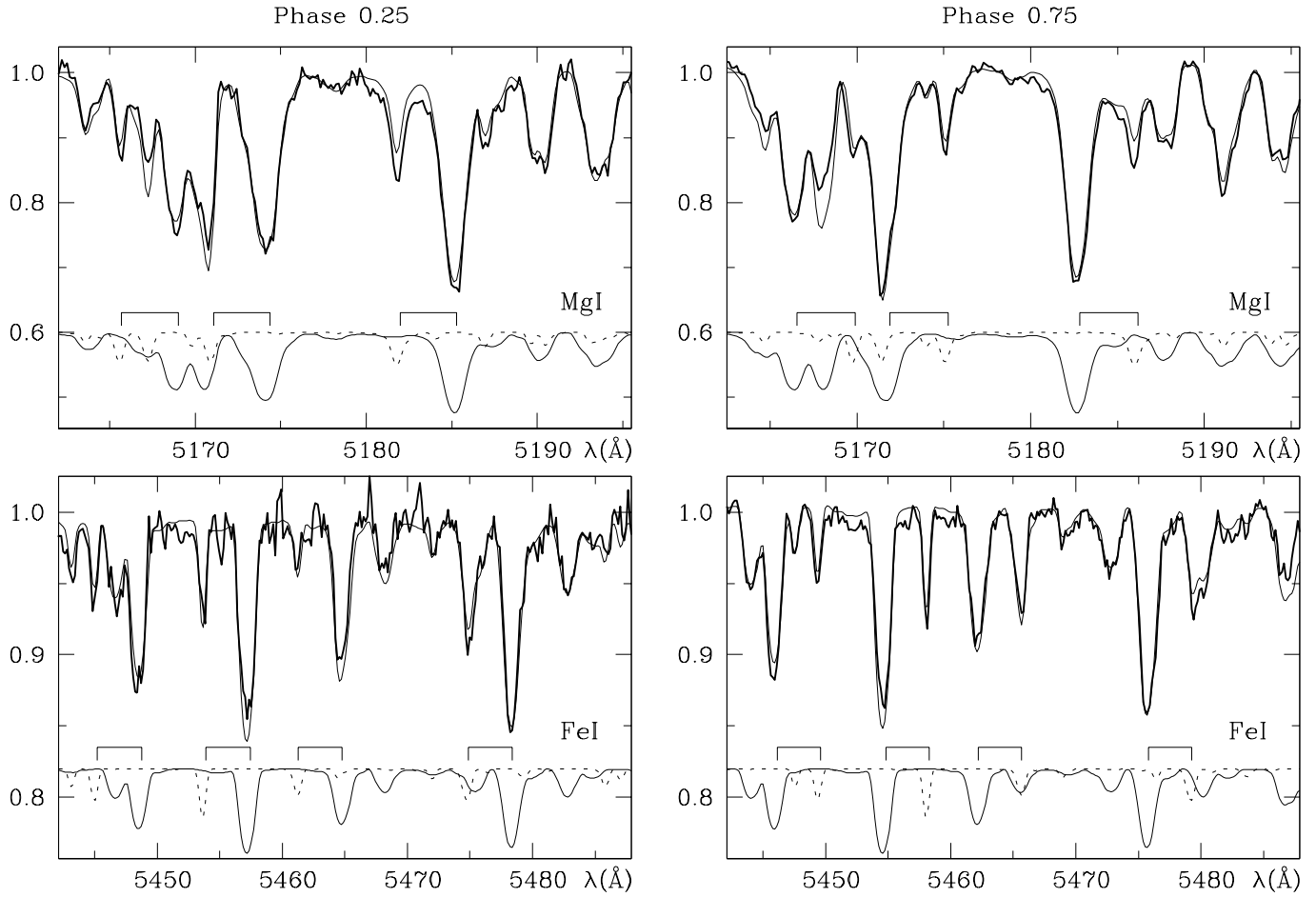


Fig. 2. Comparison between observed (thick line) and synthetic (thin line) V432 Aur spectra over two sample wavelength regions dominated by MgI lines (top) and FeI lines (bottom). Spectra at orbital phases 0.25 and 0.75 (# 39239 and 39294 in Table 1, respectively) show full split between the two components and their position interchange allow a careful check of the fit accuracy. In each panel the lower curves represent (not to scale with the main spectra but in correct proportion between them) the contribution of each component of the binary to the formation of the observed spectrum at the given phase. The markers connect the shifted wavelengths of the same sample MgI (top panels) and FeI (bottom panels) lines in the spectra of the two components of the binary.

2.4. Zeroing radial velocities

The Cassegrain-fed Asiago Echelle spectrograph is well suited for measurement of accurate radial velocities, with a stable and modest flexure pattern modeled by Munari and Lattanzi (1991), and null *spectrograph velocity* (in the sense introduced by Petrie 1963, i.e. the systematic difference between the zeros of the stellar and thorium lamp wavelength scales as due to different slit illumination and optical path). On all spectra of Table 1 we have checked and confirmed the null spectrograph velocity using night-sky emission lines (selected from the list by Osterbrock et al. 2000). The radial velocities cluster around 0.0 km sec^{-1} with a typical 0.4 km sec^{-1} dispersion.

The spectrograph flexures can affect the results because of the observing mode, and must be corrected for. Each 1800 sec spectrum on the star was followed - after the 3 min required to read the science exposure and to prepare for the thorium 3 sec exposure - by the compar-

ison spectrum with the telescope still tracking the star. In such a way, a shift of ~ 18 min in hour angle is introduced between the telescope position at mid-exposure on the star and on the thorium lamp. To account for the flexure pattern and possible off-center guiding of the stellar photo-center on the slit, the rich telluric line spectrum on the reddest orders of the recorded spectra has been cross-correlated against a template telluric spectrum, following a technique pioneered by Griffin and Griffin (1973). The template telluric spectrum has been obtained with exactly the same instrumental set-up on a fast rotating early type star observed close to zenith (where the flexure pattern flattens toward zero) with an extremely high S/N, observed so to uniformly illuminate the spectrograph slit. Measuring the flexure pattern on Echelle orders different from those where the stellar radial velocities are derived is perfectly suited because the flexure pattern and the off-center guiding are rigid shifts over the spectrograph focal

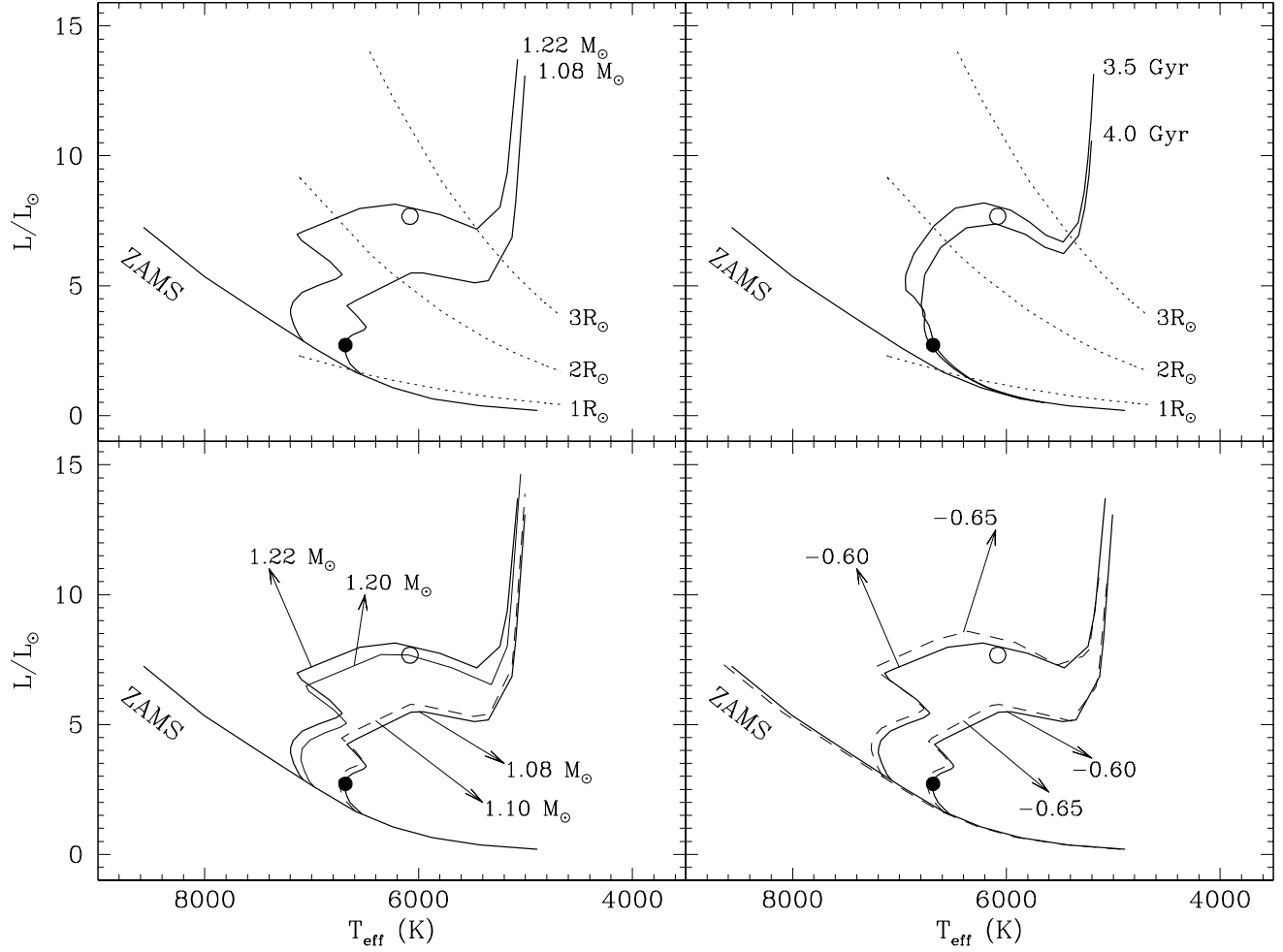


Fig. 3. Comparison between temperature and luminosity as derived from the orbital solution (cf. Table 3) and those of theoretical stellar models for the masses of the two components of V432 Aur ($1.22 M_{\odot}$ and $1.08 M_{\odot}$) at the $[Z/Z_{\odot}] = -0.6$ metallicity derived by fitting with synthetic spectra. The plotted theoretical Padova evolutionary tracks and isochrones (Fagotto et al. 1994, Bertelli et al. 1994, and follow-ups with the latest up-dates available via the web interface to the Padova theoretical group at the address <http://pleiadi.pd.astro.it/>) have been derived from interpolation of adjacent points in the computed grid ($1.00 - 1.10$ and $1.20 - 1.30 M_{\odot}$, and -0.37 and -0.67 for $[Z/Z_{\odot}]$). The agreement is excellent in both position on the tracks (upper left panel) and on the isochrones (upper right panel), the latter supporting a 3.75 Gyr age. The bottom panels show how the theoretical loci move for minimal changes in mass and metallicity, indicating the high sensitivity of the method.

plane, amounting to the same linear dimensions over the whole CCD.

The resulting combined correction for flexures and off-center guiding has typically been less than 1 km sec^{-1} , and it is already incorporated in the values reported in Table 1. The limited amplitude of these perturbing effects is due to (i) observations obtained as close as possible to meridian transit, (ii) a typical seeing matching the 2 arcsec slit width (in the FWHM sense), and (iii) long enough exposures to average out momentarily off-center guiding.

3. Orbital solution

The orbital modeling of V432 Aur has been obtained with version WD98K93d³ of the Wilson-Devinney code (Wilson and Devinney 1971) as modified by Milone et al. (1992) to include Kurucz's model atmospheres to approximate the surface fluxes of the two stars. The computations have been run within Mode-2 program option. Input parameters for the first iterations (period and epoch, semi-major axis, mass ratio, temperature of the two components, zero eccentricity, Kopal's surface potential Ω_1 and Ω_2 , bolometric albedos) have been computed by hand from radial and light curves and from spectral types of both components. They turned out to be already quite accurate be-

³ Latest code development are available via the web page <http://www.boulder.swri.edu/~terrell/talks/aavso2001/code/ebdoc98.pdf>

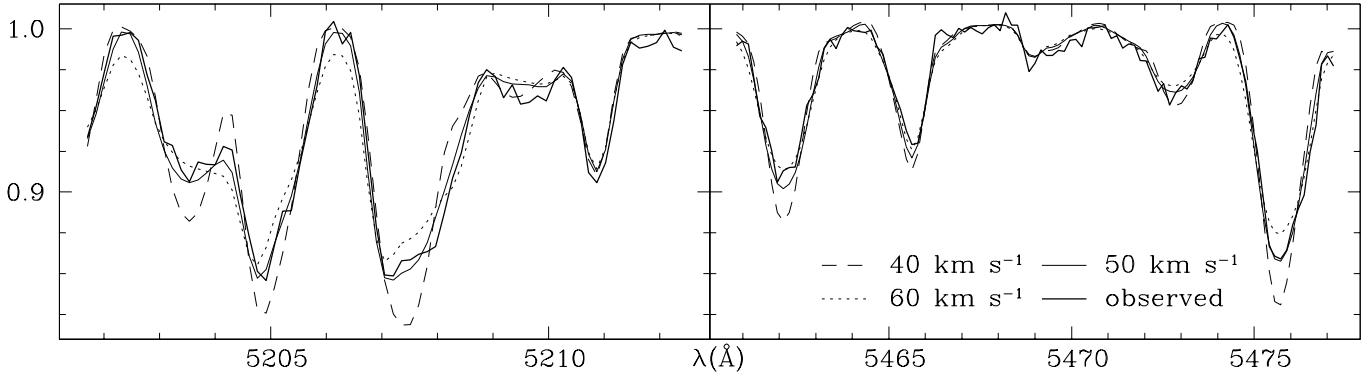


Fig. 4. Rotational velocity of the secondary star in V432 Aur. The thick line is a short wavelength range from spectrum #39294 at phase 0.75 (cf. Table 1). The thin lines, similarly to Figure 2, are the added synthetic spectra (with the proper intensity ratio and velocity shift) of the secondary and primary component. Parameters of the synthetic spectra are the same as in Table 3, except that three different rotational velocities are explored for the secondary: 40, 50 and 60 km sec^{-1} . It is evident how 40 km sec^{-1} (the co-rotation velocity) provides an under-estimate of the actual rotational velocity.

Table 4. Atmospheric parameters of V432 Aur from a χ^2 fit to the library of synthetic Kurucz's spectra of Munari et al. (2003) computed at the same resolution of the Asiago Echelle spectrograph ($R=20\,000$) and extending over 2500–10500 Å. The results from the orbital solution in Table 2 for T_{eff} and $\log g$ are given for comparison.

		χ^2 fit to synth. spectra	orbital solution
T_{eff} (K)	prim.	6750 ± 100	6685 ± 85
	sec.	6100 ± 50	6080 ± 85
$\log g$	prim.	4.25 ± 0.25	4.29 ± 0.008
	sec.	3.75 ± 0.25	3.74 ± 0.01
$V_{\text{rot}} \sin i$ (km sec $^{-1}$)	prim.	20 ± 5	
	sec.	50 ± 5	
[Z/Z $_{\odot}$]		-0.6 ± 0.05	

cause the final achieved solution converged toward pretty similar values. The reddening has been taken to be null because the observed colors well match the expectation from synthetic spectral modeling (sect.4 below) and no interstellar NaI line is visible in the spectra (to a sensitivity limit of 0.03 Å equivalent to $E_{B-V} \leq 0.01$ according to Munari and Zwitter 1997 calibration).

Limb darkening coefficients have been taken from Van Hamme (1993) interpolated for the metallicity, temperature and gravity appropriate for the components of V432 Aur. The square root law for limb darkening has been adopted as usual for radiative atmosphere, which is custom to assume for stars as the components of V432 Aur. During final iterations the coefficients for the secondary star have been slightly adjusted to achieve

the closest possible match with the light curve during primary minimum ($x_{\text{bolo}}=0.151$, $y_{\text{bolo}}=0.551$, $x_B=0.375$, $y_B=0.498$, $x_V=0.151$, $y_V=0.650$).

We checked for possible multiple reflection effects but, as expected given the wide separation of the binary components, they were found negligible and thus dropped from further modeling. Therefore only the inverse square law illumination was considered, and the bolometric albedos were set to 1.0 and tests on the lightcurve confirmed the choice.

Finally, a gravity brightening exponent $\beta=1.0$ has been adopted consistently with the radiative nature of the atmospheres in V432 Aur, and co-rotation of both components has been taken in agreement with evidences from the atmospheric spectral analysis and stability of spot longitude as discussed below.

The resulting orbital modeling and corresponding physical quantities are summarized in Table 3, and the model radial velocity and light curves are over-plotted to observed values in Figure 1. In the latter no Rossiter effect is introduced given the absence of observed radial velocities at the key short phases around primary and secondary eclipses that could be used to check it.

3.1. A surface bright spot

An evident O'Connell effect (O'Connell 1951, Davidge and Milone 1984) is present in the V432 Aur light curve centered close to 0.75 orbital phase. Noting the (a) reduction in the CaII far-red triplet line depth around phase 0.75 in the spectra of the secondary (these are lines which usually display emission cores in stars with active surfaces; Ragagni et al. 2003) and (b) the orbital modeling indicating at phase 0.75 a model brightness lower than observed by a few hundreds of a magnitude, we introduced a bright spot on the surface of the secondary that brought model and observed light curves into agreement (the model lightcurve

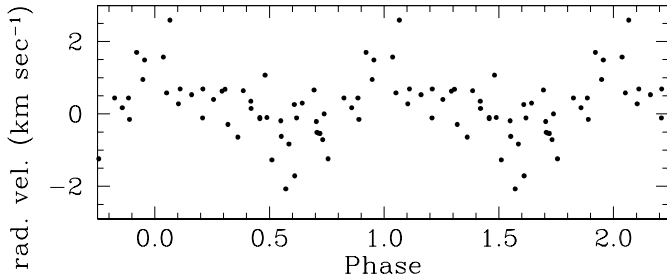


Fig. 5. δ Sct pulsation activity of the more massive, larger and cooler component of V432 Aur, phase plotted for a possible 0.1678 day period. The residuals of all the observed radial velocities of the δ Sct variable (star 2 in Table 1) from the orbital solution of Figure 1 (and Table 2) have been used.

in Figure 1 includes the effect of the spot as well as the data in Table 3).

The spot that we found bringing model and observed light curves into agreement is placed on the equator at 310° longitude on the surface of the secondary (0° toward the primary, counted in the orbital motion direction, as the convention for WD98K93 code). The spot is taken circular, with an angular extent of 12° as seen from the center of secondary star, with a 20% increase in T_{eff} with respect to the temperature of surrounding unperturbed stellar surface (7300 K). However, different combinations of temperature, angular extent and latitude still provide acceptable fits to the observed light curve. Our analysis is not aiming to precise values for the spot parameters, but just to bring attention to the fact that spot(s) are present on the surface of the secondary star of V432 Aur.

The spot has been present during the entire period of our observations, because the lightcurve around 0.75 orbital phase as displayed in Figure 1 comes from observations secured at various epochs, and all individual branches display the same O'Connell effect. In particular, the longitude of the spot appears to have remained constant during the whole observing period, indicating both stellar co-rotation and absence of spot migration.

It could be argued that the observed O'Connell effect is instead due to a *dark* spot on the other side that reduces around orbital phase 0.25 an ellipticity effect of the secondary. We are inclined to discard this possibility because a dark spot should not produce emission cores in the diagnostic CaII far-red triplet lines and because the orbital modeling above described would hardly converge in such a scenario.

4. Analysis of stellar atmospheres

The spectrum of V432 Aur at primary minimum is due only to the secondary star, and subtracting it from the spectrum at secondary eclipse would provide the spectrum of the primary component. Unfortunately, during the scheduled spectroscopic observing runs at the telescope, V432 Aur never passed through the primary eclipse, and

therefore it has not been possible to obtain the isolated spectra of the individual components.

To the aim of performing an atmospheric analysis of the two components of V432 Aur we have therefore focused on the spectra of the highest S/N around phases 0.25 and 0.75 (cf. Table 2), where the velocity separation of the components is maximum and the same lines from the two components are unblended. Working simultaneously at phase 0.25 and 0.75 allows also to get rid of line superposition and strongly reinforces the robustness of the overall fit.

To derive the basic stellar parameters (T_{eff} , $\log g$, $[Z/Z_{\odot}]$ and V_{rot}) we have performed a χ^2 best match analysis of the high S/N observed spectra around phases 0.25 and 0.75 (spectrum # 39233, 39239, 39605, 39294 and 39607 in Table 1) against the extensive grid of synthetic Kurucz's spectra computed by Munari et al. (2003) for the same resolution of the Asiago Echelle spectrograph ($R=20\,000$) over the $2\,500$ – $10\,500$ Å range (thus fully covering the wavelength range recorded for V432 Aur). The Munari et al. (2003) synthetic atlas covers the range $3\,500 \leq T_{\text{eff}} \leq 47\,500$, $0.0 \leq \log g \leq 5.0$, $+0.5 \leq [Z/Z_{\odot}] \leq -2.5$ (with solar relative abundances for metals) and $0 \leq V_{\text{rot}} \leq 500$ km sec $^{-1}$. The grid steps around the values appropriate to V432 Aur are 250 K in temperature, 0.5 dex in gravity, 0.5 dex in metallicity and 10 km sec $^{-1}$ in rotation.

To proceed independently from the orbital solution, and thus to use the atmospheric analysis to validate it, we had to first define the region where the true minimum of the χ^2 distribution has to be looked for, to avoid being trapped in unphysical local minima. To accomplish this, we have isolated from the spectrum secured at secondary eclipse (#39684 in Table 1) the wavelength range 8480–8740 Å (dominated by diagnostic CaII triplet and Paschen series lines) and we have classified it against the observed spectral atlases of Munari and Tomasella (1999) and Marrese et al. (2003) obtained over the same wavelength range with the same Asiago Echelle spectrograph, and checked it for consistency against the equivalent synthetic atlas of Munari and Castelli (2000). Having determined in ~ 6500 K the combined temperature of the two stars, we have moved to the analytical χ^2 test by fixing to 5500–7500 the temperature boundary and to ≤ 100 km sec $^{-1}$ the rotational velocities and imposing no restriction on gravity and metallicity. The analysis has been limited to the same six Echelle orders adopted for the derivation of radial velocities (cf. sect. 2.3), ready to include additional orders if not satisfactorily converging on the first six. This has not been necessary given the close similarity of the results among the 6 selected orders.

The results of the atmospheric analysis are given in Table 4, where a comparison is provided with the parameters common to the orbital solution. Given the absolute independence of the two methods (carried out independently by two distinct sub-groups of the authors of this paper), the remarkable correspondence mutually reinforce the confidence in the orbital solution and atmospheric

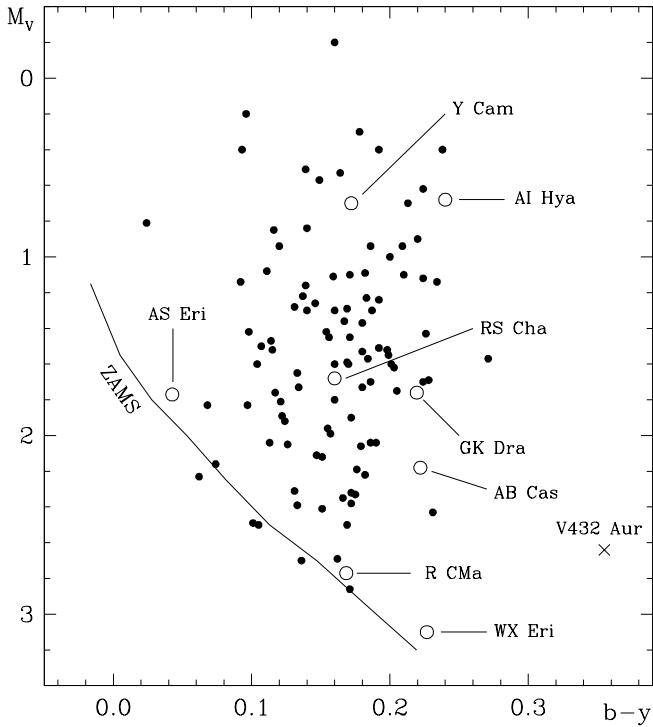


Fig. 6. Position on the HR diagram of the δ Sct component of V432 Aur compared with those given by Breger (1979). Position of δ Sct components of eclipsing binaries are plotted with open circles and identified (from Broglia & Marin 1974, Clausen & Nordström 1980, Griffin & Boffin 2003, Jørgensen & Grønbech 1978, Popper 1973, Rodríguez et al. 1998, Sarma & Abhyankar 1979, Sarma et al. 1996, Zwitter et al. 2003).

analysis. Two small and diagnostic samples of the 4860–5690 Å range investigated via χ^2 test are shown in Figure 2 to show the match between observed and synthetic spectra. Inspection of the match over the whole range does not support chemical anomalies, and therefore the metals in V432 Aur appear to follow the relative Sun proportions. If chemical anomalies should have emerged, it would have been required to run a devoted atmospheric analysis (instead of the χ^2 comparison to a pre-computed grid).

5. Comparison with stellar theoretical models

The theoretical models describe the location of stars on the *theoretical plane* L, T_{eff} , while observations place the stars on the *observational plane*, e.g. $V, (B-V)$. The correspondence between them is all but a straightforward one, being strongly affected by bolometric correction, color-temperature transformation, distance, reddening, proper knowledge of the transmission profile of the photometric bands, etc. The orbital solution in Table 2, providing directly L and T_{eff} , overcomes all such difficulties and allow an assumption-free comparison between observations and models.

Adopting $T_{\text{eff}}=5770$ K and $R=6.96 \cdot 10^6$ km for the Sun (Allen 1976), the position of the two components of

V432 Aur on the L, T_{eff} plane is presented in Figure 3, where a comparison is provided with evolutionary tracks and isochrones appropriate for the masses (1.22 and 1.08 M_{\odot}) and metallicity ($[Z/Z_{\odot}]=-0.6$) of the system components. They have been obtained via interpolation over the grid computed by the Padova theoretical group (Fagotto, et al. 1994, Bertelli et al. 1994, Girardi et al. 2000, and references therein). Given the high sensibility to mass and metallicity of the evolutionary tracks, as depicted in the lower panels of Figure 3, the excellent agreement between observations and theory is an independent check of the accuracy of the results obtained with the orbital and atmospheric analysis. The placing of both components exactly halfway between the isochrones for 3.5 and 4.0 Gyr suggests an age of 3.75 Gyr for V432 Aur.

The secondary star is well evolved away from the main sequence and approaching the base of the giant branch, while the primary has only marginally moved away from the ZAMS and is still living its main sequence phase.

6. Synchronous rotation and macro-turbulence

Given the long life lived by both components on the main sequence, there is little room for doubts that they reached at that time perfect synchronization between orbital and rotation periods. We can obviously assume that the rotation axes are aligned with the orbital axis (reached earlier in the binary evolution according to the time scale discussed by Hut 1981; for deviations from the rule see for ex. Gleboksi and Stawikowski 1997). Consequently, from the orbital period and stellar radii in Table 2 it can be derived that the equatorial rotational velocities for synchronous rotation at the present time are 20 and 40 km sec $^{-1}$ for the primary and the secondary, respectively. The rotational velocities derived by the atmospheric analysis reported in Table 3 are 20 and 50 km sec $^{-1}$ for the primary and the secondary, respectively. While the match is perfect for the primary, no doubt the line profiles for the secondary star show a broadness that if interpreted in terms of rotation would indicate the secondary to rotate *faster* than synchronous rotation, even if a precise quantification at 1 km sec $^{-1}$ level requires higher resolution spectra obtained during the totality phase at the primary eclipse. This finding is unexpected, because one may argue that an *expanding* star tends to rotate slower for obvious arguments based on the conservation of the angular momentum, and tidal torque forces can bring the star in synchronous rotation with the orbital motion only if their time scale is shorter than the expansion time-scale. The time scale for an expansion of 10% of the radius of the secondary star of V432 Aur is (from the evolutionary tracks):

$$\Gamma_{(R \uparrow 10\%)} = 6 \cdot 10^7 \text{ yr} \quad (1)$$

Following Zahn (1977) the synchronization time for stars with convective envelopes can be expressed as function of mass-ratio q and period P as:

$$t_{sync} \approx 10^4 \left(\frac{1+q}{2q} \right)^2 P^4 \text{ yr} \quad (2)$$

or $t_{sync} \sim 8 \cdot 10^5$ yr in our case, thus 2 orders of magnitude faster than radius expansion. Therefore, the evolved component of V432 Aur should currently be locked into synchronicity.

The extra broadness of spectral lines of the secondary star is probably not due to rotation but instead to a *macro-turbulent* velocity field in its atmosphere. The net effect of macro-turbulence affects mostly the wings of the lines, making them broader (cf. Grey 1992). Macro-turbulent motions on a scale larger than observed with Sun's photospheric granulation have to be expected in the secondary star of V432 Aur considering that large spots affect its surface (cf. sect. 3.1) and that it is pulsating as a δ Sct star (cf. sect 7 below). Macro-turbulent velocities determined by Donati et al. (1995) for the active surface RS CVn star λ Andromedae are $\zeta_p = 5.5 \text{ km sec}^{-1}$ for the photosphere and $\zeta_p = 10 \text{ km sec}^{-1}$ for the active surface regions.

Higher resolution observations (with a resolving power not less than 60 000) during the primary minimum are obviously desirable to better investigate the line profiles of the secondary star to the aim of disentangling the rotational from the macro-turbulence contribution to its width.

7. The δ Sct pulsation

Da02b already noted how the lightcurve of V432 Aur is affected by an additional variability superimposed to the eclipsing one. In fact, the light curves in Figure 1 show a *noise* much larger than expected for a 5 millimag-mag precision of the individual points. The flat bottom of the primary eclipse shows distinct branches corresponding to different observing epochs, which almost vanish at secondary eclipse. It is therefore clear that the additional variability is associated with the secondary, larger and cooler component.

Our photometric observations do not cover sufficiently long, uninterrupted runs to allow fruitful period search at specific epochs, and analysis of the whole data set does not provide firm values, except indications that possible periods could be found around 0.16-0.17 days. The residuals of radial velocities of the secondary from its model fitting in Figure 1 have been similarly analyzed with a deeming-Fourier code, providing a strong periodicity peak at 0.1678 day which is illustrated in Figure 5.

The amplitude of the variability is $\Delta V \approx 0.075$ mag and $\Delta RV \approx 1.5 \text{ km sec}^{-1}$, and the spectral classification of the intrinsic variable component is F9 IV. These values fall within the boundaries defining the class of δ Sct pulsating variables. According to the review by Feast (1996), their periods are shorter than 0.3 days, their spectral types go from A to F, and the amplitudes span from a few

millimag-mag up to 0.8 mag with a mean around 0.2 mag. They may be both radial or non-radial pulsators, or even display a combination of the two modes, which superposition causes a beating that makes the lightcurve to appear frequently chaotic. The shape and amplitude of the light and pulsation curves change continuously, as nicely documented by Breger (1977). Phase over-plotting of data from a range of different epochs frequently results in a wash-out of the pulsation shape of the curve, which appears disappointingly *too noisy*. As stated above, our photometric observations have been scattered through many nights, and no single observing run is densely populated and is long enough to allow to investigate pulsation light curves at any individual epoch. A long series of consecutive observations does not exist either for the radial velocities.

The scatter of radial velocities in Figure 5 is larger than that expected on the base of the individual errors (cf. last column of Table 2) and it is therefore probably a manifestation of the superposition of different shapes of the pulsation curve. A similar $0.5/1.0 \text{ km sec}^{-1}$ scatter is shown by the multi-epoch radial velocity curve of the δ Sct variable within the GK Dra eclipsing system (Dallaporta et al. 2002a, Griffin and Boffin 2003).

The properties as derived by the orbital and atmospheric analysis carried out in this paper well constrain the physical and evolutionary status of the δ Sct in V432 Aur, and if coupled to appropriate photometric and radial velocity mapping of the pulsation curve, they could be used to test current models for this type of variable. We plan for the coming new observing season to obtain night-long consecutive series of photometric (optical and possibly infrared too) and radial velocity observations aimed to map in detail the pulsation characteristics of the δ Sct in V432 Aur.

Acknowledgements. We would like to thank R. Barbon (Asiago) for assistance during the whole project, G. Bono (Rome) for useful discussion on δ Sct stars, M. Fiorucci (Perugia) for assistance with coding the χ^2 algorithm, U. Jauregi and F. Castelli for support in handling with Kurucz's spectra, and C. Boeche (Asiago) who secure a few of the spectra here discussed. R. Sordo is supported by COFIN-2001 grant.

References

- Allen, C.W. 1976, *Astrophysical Quantities*, Athlone Press, London
- Andersen, J. 1991, *A&AR*, 3, 91
- Bertelli, G., Bressan, A., Chiosi, C., Fagotto, F., Nasi, E. 1994, *A&AS* 106, 275
- Bessel, M., S. 2000, *PASP*, 112, 961
- Breger, M. 1977, *PASP*, 89, 339
- Breger, M. 1979, *PASP*, 91, 5
- Broglia, P., & Marin, F. 1974, *A&A*, 34, 89
- Caldwell, J. A. R., Cousins, A. W. J., Ahlers, C. C., van Wamelen, P., & Maritz, E. J. 1993, *SAAO Circ.*, 15, 1
- Clausen, J. V., & Nordström, B. 1980, *A&A*, 83, 339
- Dallaporta, S., Tomov, T., Zwitter, T., Munari U. 2002a, *IBVS* 5312

- Dallaporta, S., Tomov, T., Zwitter, T., Munari U. 2002b, IBVS 5319
- Davidge, T.J., and Milone, E.F. 1984. AJ, 55, 571
- Donati, J.-F., Henry, G.W., Hall, D.S. 1995, A&A 293, 107
- Fagotto, F., Bressan, A., Bertelli, G., & Chiosi, C. 1994, A&AS, 104, 365
- Feast, M. W. 1996, in Light Curves of Variables Stars, A Pictorial Atlas, Sterken & Jaschek eds., pp 81
- Girardi, L., Bressan, A., Bertelli, G., Chiosi, C. 2000, A&AS 141, 371
- Glebocki, R., Stawikowski, A. 1997, A&A 328, 579
- Gray, D.F. 1992, The Observations and Analysis of Stellar Photospheres, Cambridge Univ. press
- Griffin, R.F., & Griffin, R. 1973, MNRAS, 279, 108
- Griffin R.F., Boffin, H.M.J. 2003, The Observatory, in press (astro-ph/0306107)
- Hut, P. 1981, A&A 99, 126
- Jørgensen, H. E., & Grønbech, B. 1978, A&A, 66, 377
- Kurtz M.J., Mink D. J. 1998, PASP, 110, 934
- Kurucz, R. L. 1979, ApJS, 40, 1
- Latham, D.W., Stefanik, R.P., Torres, G.D., Robert J., Mazeh, T., Carney, B.W., Laird, J.B., Morse, J.A. 2002, AJ 124, 1144
- Marrese, P. M., Boschi, F., Munari, U. 2003, A&A, 406, 995
- Milone, E.F., Stagg, C.R., Kurucz, R.L. 1992, ApJS 79, 123
- Munari, U., & Lattanzi, M. G. 1992, PASP, 104, 121
- Munari, U., Zwitter, T. 1997, A&A 318, 269
- Munari, U., & Tomasella, L. 1999, A&AS, 137, 521
- Munari, U., & Castelli, F. 2000, A&AS, 141, 141
- Munari, U., Tomov, T., Zwitter, T., Milone, E. F., Kallrath, J., Marrese, P.M., Boschi, F., Prša, A., Tomasella, L., & Moro, D. 2001, A&A, 378, 477
- Munari, U., Zwitter, T., Sordo, R., Castelli, F. 2003, A&A, to be submitted
- O'Connell, D.J.K. 1951, Pub. of the Riverview College Obs., 2, 85.
- Osterbrock, D. E., Waters, R. T., Barlow, T. A., Slanger, T.G., & Cosby, P.C. 2000, PASP, 112, 733
- Petrie, R. M. 1963, in Basic Astronomical Data, K.A. Strand ed., pp 64
- Popper, D. M. 1973, ApJ, 185, 265
- Ragaini, S., Andretta, V., Gomez, M. T., Terranegra, L., Busà, I., & Pagano, I. 2003, in GAIA Spectroscopy, Science and Technology, U.Munari ed., ASP Conf. Ser. 298, pp 461
- Rodríguez, E. 2002, in Stellar Structure and Habitable Planet Finding, B.Battrick ed., ESA Publications Division, pp 323
- Rodríguez, E., Claret, A., Sedano, J. L., García, J. M., & Garrido, R. 1998, A&A, 340, 196
- Sarma, M. B. K., & Abhyankar, K. D. 1979, Ap&SS, 65, 443
- Sarma, M. B. K., Vivekananda Rao, P., & Abhyankar, K. D. 1996 ApJ, 458, 371
- Straižys, V., & Kurieliene, G. 1981, Vilnius Obs. Bull., 56, 25
- Tonry J., Davis M. 1979, AJ, 84, 1511
- van Hamme, W. 1993, AJ, 106, 2096
- Wilson, R. E., & Devinney, E. J. 1971, ApJ, 166, 605
- Zahn, J. -P. 1977, A&A, 57, 383
- Zucker S., Mazeh T. 1994, ApJ, 420, 806
- Zwitter, T., Munari, U., Marrese, P.M., Prša, A., Milone, E. F., Boschi, F., Tomov, T., & Siviero, A. 2003, A&A, 404, 333